Three-Dimensional Large-Scale Aerodynamic Shape Optimization Based on Shape Calculus

4 authors, including:

Volker H. Schulz
Universität Trier
156 PUBLICATIONS **3,080** CITATIONS

Three Dimensional Large Scale Aerodynamic Shape Optimization based on Shape Calculus

Stephan Schmidt[*] and Volker Schulz[†]

University of Trier, Universitätsring 15, 54296 Trier, Germany

Caslav Ilic[‡]

German Aerospace Center (DLR), Lilienthalplatz 7, 38108 Braunschweig, Germany

Nicolas R. Gauger[§]

RWTH Aachen University, Schinkelstr. 2, 52062 Aachen, Germany

Large scale three dimensional aerodynamic shape optimization based on the compressible Euler equations is considered. Shape calculus is used to derive an exact surface formulation of the gradients, enabling the computation of shape gradient information for each surface mesh node without having to calculate further mesh sensitivities. Special attention is paid to the applicability to large scale three dimensional problems like the optimization of an Onera M6 wing or a complete blended wing-body aircraft. The actual optimization is conducted in a one-shot fashion where the tangential Laplace-operator is used as a Hessian approximation, thereby also preserving the regularity of the shape.

Nomenclature

γ Adiabatic exponent

α Angle of attack

q Design vector

κ Additive mean curvature

Δ_Γ Laplace–Beltrami operator

$\delta_{i,k}$ Kronecker symbol

ρ Density

E Total energy

ℓ Scalar constraints, e.g. lift or structural constraints

ϵ Smoothing parameter

Γ Unknown boundary to be optimized

Γ_0 Euler slip wall, i.e. the aircraft surface

a Rotation of the coordinate system

[*]Dr. S. Schmidt, Department of Mathematics, Stephan.Schmidt@uni-trier.de
[†]Prof. Dr. V. Schulz, Department of Mathematics, Volker.Schulz@uni-trier.de
[‡]Dipl.-Ing. C. Ilic, CASE, caslav.ilic@dlr.de
[§]Prof. Dr. N. R. Gauger, Computational Mathematics Group, gauger@mathcces.rwth-aachen.de

American Institute of Aeronautics and Astronautics

λ Adjoint variable

$\mathcal{L}$ Lagrangian

μ Adjoint variable for vector constraints

n Outer normal

ν Adjoint variable for scalar constraints

Ω Domain occupied by the fluid

p Pressure

y State vector

$\tilde{D}_x z$ Reduced Jacobian of quantity z with respect to x

U Vector of conserved variables

V Smooth vector field prescribing the deformation direction

u Velocity vector

A_i Euler Flux Jacobian matrices

B Reduced Hessian

c Vector contraints, e.g. flow solver residual

C_D Drag coefficient

C_L Lift coefficient

C_P Pressure coefficient

$D_x z$ Jacobian of quantity z with respect to x

$dz[V]$ Material derivative of quantity z in direction V

f Objective function, standard optimization problem

g Shape gradient

H Enthalpy

$H_{z_1 z_2}$ Second partial derivative of the objective with respect to z_1 and z_2

I Identity matrix

J Objective function, shape optimization problem

T_t Bijective family of mappings applying the shape deformation

U_H Conserved variables with enthalpy as last component

x_1 Coordinate axis, chord direction

x_2 Coordinate axis, span direction

x_3 Coordinate axis, thickness direction

$z'[V]$ Shape derivative of quantity z in direction V

I. Introduction

Applied aerodynamic shape optimization, especially for industry size problems, has in the past almost always followed a parametric approach, meaning that parts of the aircraft like the wing cross-sections are deformed by adding smooth ansatz functions such as the popular Hicks–Henne functions[1] to the geometry. Other approaches frequently encountered for CAD-free fully three dimensional parameterizations are for example perturbing the control points of spline surfaces or free-form deformations. All of these approaches have in common that the actual optimization problem is considered post parameterization, meaning the gradient is computed according to the standard Lagrange formula

$$\frac{dJ}{dq} = \frac{\partial J}{\partial q} - \lambda^T \frac{\partial c}{\partial q},\tag{1}$$

where λ is the corresponding adjoint variable solving

$$\left[\frac{\partial c}{\partial y}\right]^T \lambda = \frac{\partial J}{\partial y}.\tag{2}$$

The adjoint flow solver is therefore independent of the shape optimization nature of the problem as only the derivatives with respect to the flow states are needed. However, in order to construct the gradient out of the primal and adjoint states, the parameterization of the shape must be considered. Especially the term $\frac{\partial c}{\partial q}$ requires knowledge of the sensitivity of the flow solver residual with respect to mesh nodes positions effected by the parameterization q. While this approach is known to be applicable and well working, one is often forced into finite differencing for these terms.[2,3] This often makes very fine parameterizations such as using the mesh node positions itself rather impractical if not prohibitive, as the time to compute the adjoint flow solution is indeed independent of the number of design parameters, but the gradient computation actually is not. While it is possible to counter this problem by introducing another adjoint for the mesh deformation, using e.g. algorithmic differentiation on the mesh deformation tools in reverse mode[4] or a continuous approach,[5] special care must be taken not to run into memory limitations by considering the entire design chain at once, as usually the resulting gradient expression is not an exclusive surface quantity.

The alternative is to treat the problem in a non-parametric fashion. In the past, non-parametric approaches have been used to derive optimal shapes for certain flow situations on a theoretical level. For example in[6,7] a rugby-ball like shape is shown to be optimal for creeping Stokes flows, while in[8] optimality of the so-called Sears–Haack body for inviscid compressible flow is shown. Non-parametric approaches can also be found in,[9,10] but they are hardly used for any actual computations. The idea considered in the present work is to use shape calculus to differentiate the aerodynamic forces directly with respect to the input geometry, thereby arriving at a form of equation (1), which is specific for shape optimization problems and does not need explicit knowledge of the problematic partial derivatives. Shape calculus or shape sensitivity analysis describes the mathematical topic when the shape of a domain is the unknown. Pioneered in,[11,12] it can be used to arrive at exact surface formulations of the gradients for shape optimization problems, which is often termed the Hadamard form

$$dJ(\Gamma) = \int_\Gamma \langle V, n \rangle \; g \; dS.\tag{3}$$

Once g is known, a steepest descent algorithm can easily be conducted according to

$$\Gamma^{k+1} := \{x + \tau g(x)n(x) : x \in \Gamma^k\},$$

where τ is the step-length of the algorithm. Therefore, using the surface mesh node positions is a natural choice and furthermore, the deformation of the volume mesh is completely removed from the derivative chain. While the volume mesh nodes must of course still be somehow adapted to the new surface geometry, the derivative of the mesh deformation and the variation of the flow residual with respect to the design are not required for an exact gradient evaluation because they are included in g on an analytic level. There are previous works in aerodynamic shape optimization that use all surface mesh node positions,[13] but usually the considerable overhead in computing the gradient based on formula (1) has made this approach very inefficient.[14]

American Institute of Aeronautics and Astronautics

Here, the shape gradient g is used in a one-shot optimization strategy similar to.[15, 16] Being a reduced SQP method, one-shot depends on a proper approximation of the reduced Hessian, for which the surface or tangential Laplace operator is used. Pseudo-differential operator symbol calculus conducted in[17, 18] suggest using a Hessian approximation based on an anisotropic operator with anisotropies in chord and span direction would be best, but we found isotropic diffusion to be working very well also. Sometimes called gradient smoothing or Sobolev gradient method, similar techniques have been used in[19, 20] as a means to preserve the regularity of the aircraft shape.

While the applicability to two dimensional airfoil optimizations using the compressible Euler equations has been previously considered in,[21, 22] the aim of this paper is to study the applicability to large scale three dimensional problems. To this end, the optimization of both the Onera M6 wing as well as the optimization of a complete blended wing-body aircraft is shown. Special emphasis also lies on the correct computation of the respective surface quantities needed for evaluating the shape derivative on triangulated unstructured surface meshes. Further considerations for the incompressible Navier–Stokes equations can be found in.[21, 23, 24] Potential flow inverse design is considered in.[25]

II.   Shape Calculus

II.A.   Problem Introduction: Aerodynamic Forces

A very brief review of shape calculus is given next. More details on shape sensitivity analysis in general can be found in.[11, 12] The inviscid fluid forces acting on the aircraft surface Γ_0 are given by

$$J(U, \Omega) = \int_{\Gamma_0} \langle p \cdot a, n \rangle \ dS, \tag{4}$$

where $U := (\rho, \rho u, \rho E)$ are the conserved Euler state variables with ρ being the density, $u = (u_1, u_2, u_3)^T$ is the velocity vector, and E is the total energy of the fluid. Furthermore, the pressure p is linked to the conserved state variables by the prefect gas law

$$p = (\gamma - 1)\rho \left(E - \frac{1}{2}\|u\|^2 \right)$$

with $\gamma \approx 1.4$ being the adiabatic exponent of air. The normal to the aircraft surface is denoted by n and a is the rotation of the coordinate system, meaning for an angle of attack α, choosing

$$a_D := (\cos \alpha, 0, \sin \alpha)^T$$

leads to J being the aerodynamic inviscid pressure drag force. Similarly, chosing a as

$$a_L := (-\sin \alpha, 0, \cos \alpha)^T$$

will result in J being the lift force. In the following, it is thus sufficient to consider surface functionals only. Also, lift and drag forces do not need to be treated separately.

II.B.   Shape Calculus for Surface Functionals

A finite deformation of the aircraft surface is thought to be given by

$$\Gamma_0^t := T_t(\Gamma_0) = \{T_t(x) : x \in \Gamma_0\},$$

where T_t is a family of bijective mappings usually given by either the perturbation of identity

$$T_t(x) = x + tV(x)$$

or the speed method

$$\frac{\partial x}{\partial t} = V(t, x), \ x(0) = x_0 \in \Gamma_0.$$

American Institute of Aeronautics and Astronautics

Thus, the actual perturbation direction is given by the vector field V. For first order calculus, both the perturbation of identity and the speed method are known to be equivalent.[11, 12] Assuming enough regularity such that the chain rule holds, the preliminary shape derivative of (4) is given by

$$
dJ(U)[V] = \left[\frac{d}{dt}\bigg|_{t=0} \int_{\Gamma_0^t} \langle p \cdot a, n \rangle \ dS_t \right] + \int_{\Gamma_0} \langle p \cdot a, dn[V] \rangle \ dS + \int_{\Gamma_0} \langle p'[V] \cdot a, n \rangle \ dS. \tag{5}
$$

Using standard shape differentiation techniques and tangential calculus,[11, 12, 21, 22] one arrives at

$$
\frac{d}{dt}\bigg|_{t=0} \int_{\Gamma_0^t} \langle p \cdot a, n \rangle \ dS_t = \int_{\Gamma_0} \langle V, n \rangle \left[\left\langle \frac{\partial p}{\partial n} \cdot a, n \right\rangle + \kappa \langle p \cdot a, n \rangle \right] \ dS \tag{6}
$$

for the first term in (5). Using the same techniques, one can also arrive at

$$
\int_{\Gamma_0} \langle p \cdot a, dn[V] \rangle \ dS = \int_{\Gamma_0} \langle V, n \rangle \left[\text{div}_\Gamma \left(p \cdot a \right) - \kappa \langle p \cdot a, n \rangle \right] \ dS, \tag{7}
$$

where div_Γ is the surface or tangential divergence operator.

II.C. Shape Calculus for the Local Shape Derivative of the State Equation

Adjoint calculus must now be used to remove the local shape derivative of the pressure $p'[V]$ in (5), which will be conducted analogously to.[26, 27] Let the local shape derivatives of the conserved variables be given by

$$
U'[V] = (\rho'[V], (\rho u)'[V], (\rho E)'[V])^T.
$$

They satisfy the linearized Euler equations given by

$$
\frac{\partial}{\partial x_1} \left(A_1 U'[V] \right) + \frac{\partial}{\partial x_2} \left(A_2 U'[V] \right) + \frac{\partial}{\partial x_3} \left(A_3 U'[V] \right) = 0 \tag{8}
$$

inside the flow domain. Letting λ solve the adjoint compressible Euler equations

$$
-A_1^T \frac{\partial}{\partial x_1} \lambda - A_2^T \frac{\partial}{\partial x_2} \lambda - A_3^T \frac{\partial}{\partial x_3} \lambda = 0 \text{ in } \Omega,
$$

integration by parts in (8) shows that

$$
0 = \int_{\partial \Omega} \sum_{k=1}^3 \lambda n_k A_k U'[V] \ dS.
$$

As discussed in[26, 27] and given proper farfield adjoint boundary conditions, the relation

$$
0 = \int_{\Gamma_0} \lambda \sum_{k=1}^3 n_k A_k U'[V] \ dS = \int_{\Gamma_0} \lambda U_H \langle u'[V], n \rangle + (\lambda_2, \lambda_3, \lambda_4) n p'[V] \ dS \tag{9}
$$

holds, where U_H is given by

$$
U_H := (\rho, \rho u_1, \rho u_2, \rho u_3, \rho H)^T.
$$

Due to the fluid velocity satisfying the Euler slip boundary condition

$$
\langle u, n \rangle = 0
$$

on the aircraft surface, the local shape derivative of the velocities are then correspondingly given by

$$
\langle u'[V], n \rangle = -\langle V, n \rangle \left\langle \frac{\partial u}{\partial n}, n \right\rangle - \langle u, dn'[V] \rangle.
$$

For more details see.[21,22] Inserting this into (9), one arrives at

$$0 = \int\limits_{\Gamma_0} -\langle V, n \rangle \lambda U_H \left\langle \frac{\partial u}{\partial n}, n \right\rangle - \lambda U_H \langle u, dn[V] \rangle + (\lambda_2, \lambda_3, \lambda_4) n p'[V] \; dS.$$

Adding the above to the preliminary gradient (5) and using (6) but not yet (7), one can see that

$$dJ(U)[V] = \int\limits_{\Gamma_0} \langle V, n \rangle \left[\frac{\partial p}{\partial n} \langle a, n \rangle + \kappa p \langle a, n \rangle - \lambda U_H \left\langle \frac{\partial u}{\partial n}, n \right\rangle \right]$$
$$+ \langle pa - \lambda U_H u, dn[V] \rangle + p'[V] \left[\langle a, n \rangle + (\lambda_2, \lambda_3, \lambda_4) n \right] \; dS.$$

If the adjoint boundary condition

$$(\lambda_2, \lambda_3, \lambda_4) \, n + \langle a, n \rangle = 0$$

is satisfied on the wing, the gradient will further simplify to

$$dJ(U)[V] = \int\limits_{\Gamma_0} \langle V, n \rangle \left[\frac{\partial p}{\partial n} \langle a, n \rangle + \kappa p \langle a, n \rangle - \lambda U_H \left\langle \frac{\partial u}{\partial n}, n \right\rangle \right] \tag{10}$$
$$+ \langle pa - \lambda U_H u, dn[V] \rangle \; dS.$$

This especially means that existing adjoint flow solvers need not be modified to be useable for the computation of non-parametric shape derivatives, because both the adjoint field equation and the boundary conditions stay the same as in the classical approach. Using now also (7), one arrives at

$$dJ(U)[V] = \int\limits_{\Gamma_0} \langle V, n \rangle \left[\frac{\partial p}{\partial n} \langle a, n \rangle - \lambda U_H \left\langle \frac{\partial u}{\partial n}, n \right\rangle + \text{div}_\Gamma \; (pa - \lambda U_H u) \right] \; dS, \tag{11}$$

which is the final form of the gradient.

Comparing (10) with (11) one can see that the final Hadamard form of the gradient requires the evaluation of the tangential divergence operator on the unstructured surface mesh of the aircraft, but this can be traded for the computation of the mean curvature κ and the variation of the normal $dn[V]$. Due to more literature being available concerning mesh curvature of unstructured triangulated surfaces and the normal variation $dn[V]$ being quite easily computable on a discrete level, the latter approach was chosen.

As discussed in,[21] the variation $dn_T[V_k](x_k)$ of the face normal n_T in direction $V_k(x_i) = n(x_k)\delta_{i,k}$ with linear interpolation in-between surface mesh nodes is given by

$$dn_T[V_k](x_k) = \frac{n_k \times (x_i - x_{i+1})}{|T|},$$

where T is the surface triangle patch centered around node x_k with vertices x_i. The normal at the node x_k is denoted by $n_k = n(x_k)$. The mean curvature κ of the surface mesh is computed as described in.[28]

III.   One-Shot Optimization and Hessian Approximation

III.A.   Overview of the One-Shot Method

In order to motivate the one-shot method, a standard minimization problem is considered:

$$\min_{(y,q)} f(y, q)$$
$$\text{subject to}$$
$$c(y, q) = 0$$
$$\ell(y, q) = 0,$$

American Institute of Aeronautics and Astronautics

where $c(y, q) = 0$ refers to the flow solution residual beeing zero and $\ell(y, q) = 0$ means that additional constraints such as lift, volume, or bending stiffness are kept. Using Newton's method to solve the necessary optimality conditions of the above problem, the system

$$
\begin{bmatrix}
H_{yy} & H_{yq} & (D_y c)^T & (D_y \ell)^T \\
H_{qy} & H_{qq} & (D_q c)^T & (D_q \ell)^T \\
D_y c & D_q c & 0 & 0 \\
D_y \ell & D_q \ell & 0 & 0
\end{bmatrix}
\begin{pmatrix}
\Delta y \\
\Delta q \\
\Delta \mu \\
\Delta \nu
\end{pmatrix}
=
\begin{pmatrix}
-\nabla_y \mathcal{L} \\
-\nabla_q \mathcal{L} \\
-c \\
-\ell
\end{pmatrix},
$$

needs to be solved with the actual design update given by

$$
(y_{k+1}, q_{k+1}, \mu_{k+1}, \nu_{k+1})^T = (y_k, q_k, \mu_k, \nu_k)^T + (\Delta y, \Delta q, \Delta \mu, \Delta \nu)^T.
$$

Here, $\mathcal{L}$ denotes the Lagrangian. Assuming there exists an approximation of the Hessian of the form

$$
\begin{bmatrix}
H_{yy} & H_{yq} \\
H_{qy} & H_{qq}
\end{bmatrix}
\approx
\begin{bmatrix}
0 & 0 \\
0 & B
\end{bmatrix}
$$

and further assuming $(D_y c)^{-1}$ exists, a block Gauss-elimination and replacing $\Delta \nu$ with $\nu_{k+1} = \nu_k + \Delta \nu$ results in the system

$$
\begin{bmatrix}
B & \tilde{D}_\ell \\
(\tilde{D}_\ell)^T & 0
\end{bmatrix}
\begin{pmatrix}
\Delta q \\
\nu_{k+1}
\end{pmatrix}
=
\begin{pmatrix}
-\tilde{D}_f \\
-\ell + \lambda_\ell c
\end{pmatrix}.
\tag{12}
$$

In the context of a standard minimization problem, the reduced gradient $\tilde{D}_f$ of the objective function is given by

$$
\tilde{D}_f = \nabla_q f - (D_q c)^T (D_y c)^{-T} \nabla_y f,
$$

with an analogous definition of the reduced gradient $\tilde{D}_\ell$ of the scalar constraints. Here, however, the respective shape derivatives will be used directly for $\tilde{D}$, resulting in a shape one-shot method.

An additional aspect of the one-shot method, not directly visible in (12), is the fact that the state and adjoint flow variables are usually computed by an iterative flow solver. This usually results in any optimization procedures essentially becoming a two loop approach: An outer optimization loop with several inner loops for the primal and respective adjoint iterative flow solvers. For the problems considered here, this two loop approach is broken up by only performing a limited number of solver and adjoint iterations to compute the derivatives needed in (12). Thus, optimality of the design and feasibility of the flow state is computed simultaneously, thereby greatly reducing the wall-clock runtime.

III.B.   Hessian Approximation

Crucial for the performance of one-shot is having a good approximation of the reduced Hessian operator B. A natural choice would be the shape Hessian of the problem. However, shape Hessians are fairly complex objects even for moderate problems. While they have been successfully used in solving shape optimization problems numerically,[29, 30] it is often much more convenient to use a suitable approximation, especially in cases where the Hessian is not positive definite away from the optimum.

An analysis of the operator symbol of the Hessian for the Euler shape optimization problem conducted in[17, 18] suggests it is best to approximate the Hessian by an anisotropic operator in chord and span direction, where chord-wise, the Hessian closely resembles a diffusive operator like the Laplacian. Due to this fact and the previous successes of gradient smoothing techniques,[19, 20] we approximate the Hessian according to

$$
B \approx -\epsilon \Delta_\Gamma + I,
\tag{13}
$$

where Δ_Γ is the tangential Laplace operator on the curved two dimensional aircraft surface mesh and I is the identity. Further studies of shape Hessians for a variety of other fluid dynamics problems can be found in.[23, 25] During computation, the tangential Laplacian is computed as described in.[31] The effects of this preconditioning on the drag gradient of the Onera M6 wing can be seen in figure 1. As discussed in[21, 25] on an experimental level, such a Hessian approximation has the potential for mesh independent optimization convergence.
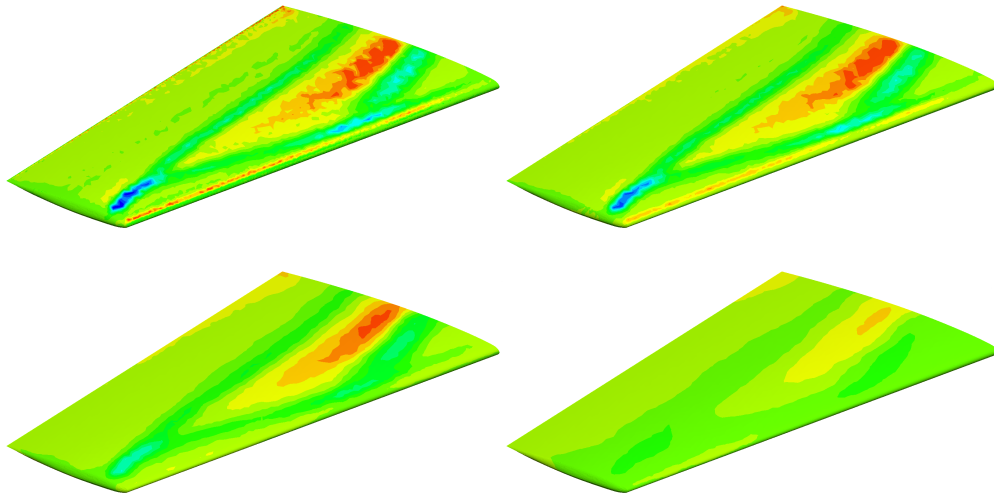
American Institute of Aeronautics and Astronautics

Figure 1. Effects of the Laplace–Beltrami preconditioner (13) **on the drag gradient for** $\epsilon = 0, 10^{-2}, 10^{-1}, 10^{0}$ **on the Onera M6 wing.**

IV.   Onera M6

The first problem under consideration is the shape optimization of an Onera M6 wing at cruise condition of Mach 0.83 and 3.01° angle of attack. In this configuration, the computed lift coefficient is $C_L = 2.762 \cdot 10^{-1}$, which is to be kept constant. The inital drag coefficient is given by $C_D = 1.058 \cdot 10^{-2}$. Primal and adjoint flow state are computed using vertex centered finite volumes with the DLR flow solver TAU. The mesh consists of $18,285$ surface mesh nodes. Since the volume mesh is perturbed using the algebraic mesh deformation tool that is part of the TAU suite, the planform had to be fixed as otherwise the deformation tool was very often unable to make volume meshes of satisfying quality. Due to this reason, the surface mesh nodes were also moved in x_3-direction only, meaning the gradient was evaluated according to equation (10) for a movement of each node in direction of the normal in the current optimization iteration at that node. However, before any actual mesh deformation is applied, there is a projection of this gradient with respect to a movement in x_3-direction only. We therefore expect a better performance of formula (10) when more sophisticated mesh deformation tools are available. Fixing the planform reduces the effective number of unknowns for the shape to $16,792$. Since most inviscid meshes feature a numerically sharp trailing edge with potentially infinite curvature, any possible problems stemming from this point are therefore also circumvented. Counting the field nodes also, there are $541,980$ unknowns for the Euler fluid state. In order to prevent a degeneration of the shape, the total volume is to be kept constant in addition to preserving the lift coefficient.

Initial and optimized airfoil cuts are shown in figure 4 and the respective C_P distributions are shown in figure 3. The optimized Onera M6 wing has a drag coefficient of $C_D = 7.567 \cdot 10^{-3}$, which corresponds to an improvement of 28.47%. Also, the optimized wing has a lift coefficient of $C_L = 2.723 \cdot 10^{-1}$, which means the lift was preserved up to 1.41%. The optimal solutions where found after 70 one-shot iterations with 10 inner iterations in each adjoint flow solver and 20 iterations in the primal. Looking at the pressure distributions in figure 3, one can see that the optimized wing is indeed shock free over the complete span. Since the cross-sectional thickness of each airfoil was not fixed, but only the total volume of the wing, one can see that the optimized wing has become thinner at the root and thicker towards the tip, which is less than prefect from a structural point of view. However, a similar shift of thickness to the tip did not occur for the VELA case and there was no mathematical constraint to account for structural requirements, making this acceptable for the purpose of the present work.

V.   VELA Blended Wing-Body

The second test is the optimization of the "Very Efficient Large Aircraft (VELA)", a blended wing-body concept. The tetrahedral mesh consists of $115,673$ surface mesh points, of which $113,956$ remain as design unknowns after fixing the planform. The mesh has a total number of $1,061,433$ nodes in the field. The flow and both the adjoints for lift and drag are again computed using the DLR flow solver TAU. As in the Onera
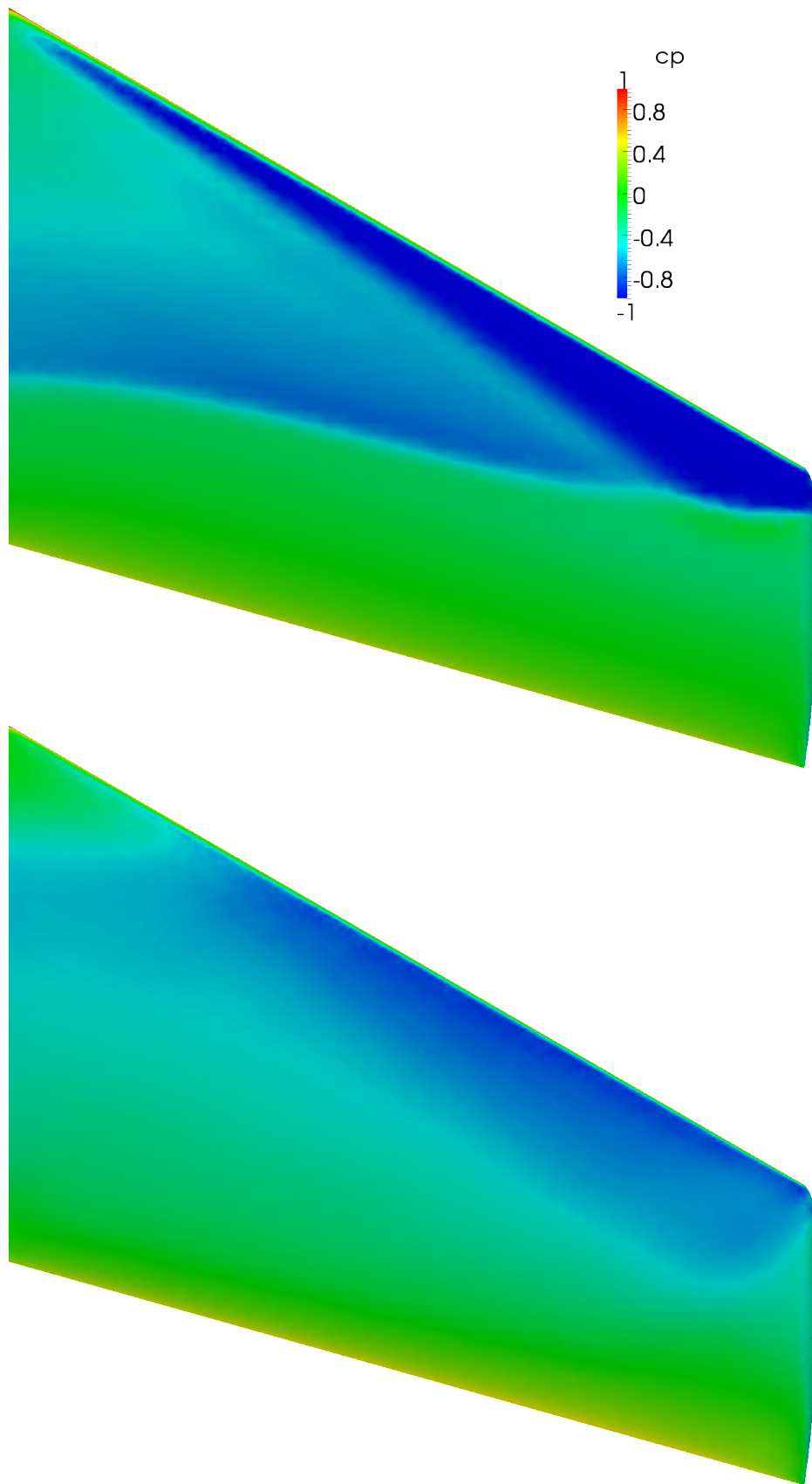
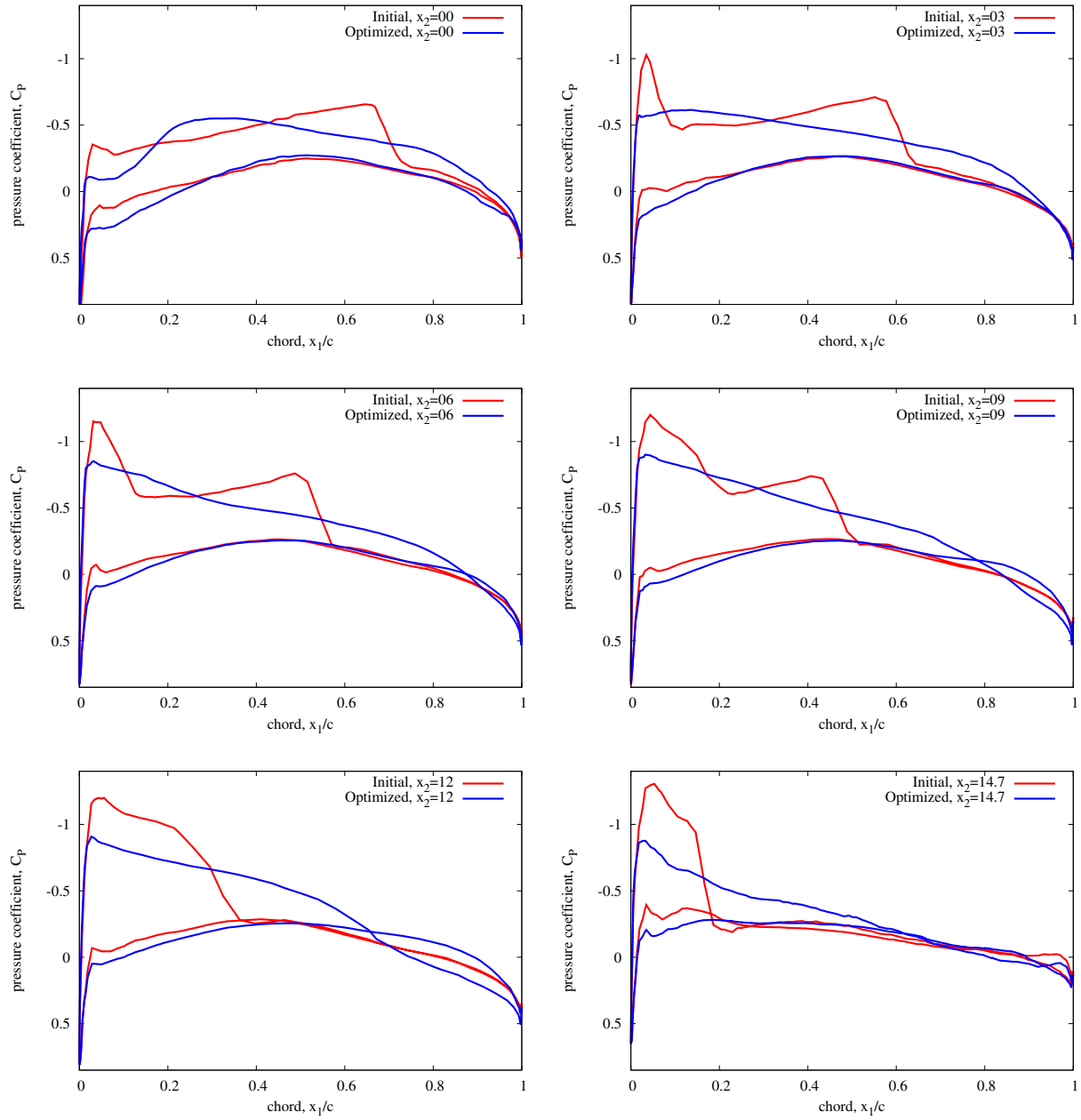**Figure 2. Initial and optimized Onera M6 wing.**

American Institute of Aeronautics and Astronautics

Figure 3. Pressure distributions across airfoil cuts for the initial and optimized Onera M6 wing. Total span wise extend is $x_2 \in [0, 15.2]$.
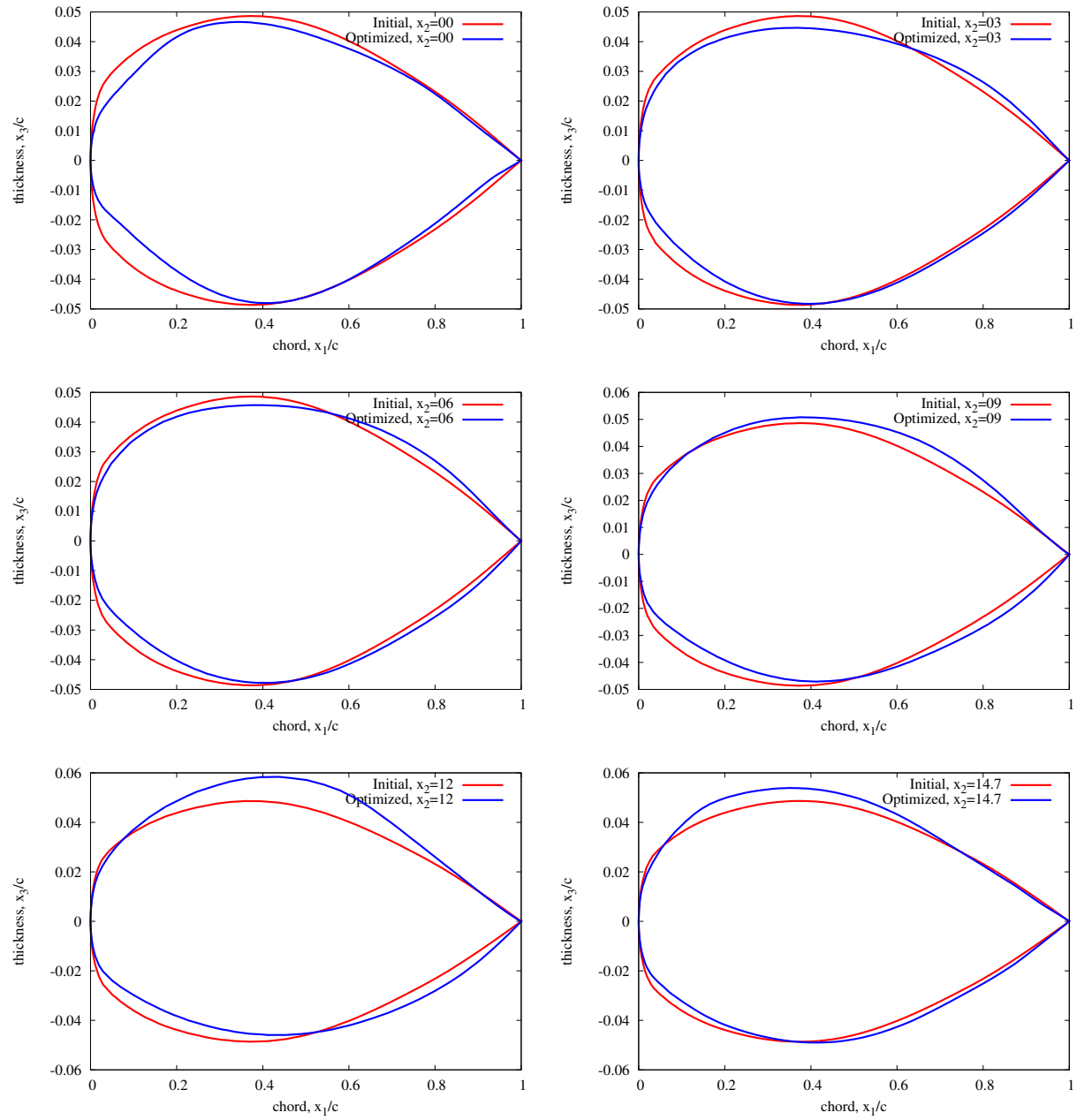
American Institute of Aeronautics and Astronautics

Figure 4. Airfoil cuts for the initial and optimized Onera M6 wing. Total span wise extend is $x_2 \in [0, 15.2]$.

American Institute of Aeronautics and Astronautics

M6 case, the gradient is again computed according to equation (10). After one update of the aircraft surface, the new volume mesh is created by deforming the mesh from the previous iteration using the algebraic mesh deformation tool that is part of the TAU software. Due to this tool having difficulties in deforming the volume mesh for perturbations of the type $V_k(x_i) = n(x_k)\delta_{i,k}$ with linear interpolation in between points, the gradient is again projected for a movement in x_3-direction only.

The initial and optimized aircraft is shown in figure 5. Some C_P plots are shown in figure 6 while the respective airfoil cross-sections are presented in figure 7. At 1.8° angle of attack and a cruise condition of Mach 0.85, the initial configuration has a drag coefficient of $C_D = 4.770 \cdot 10^{-3}$ and a lift coefficient of $C_L = 1.787 \cdot 10^{-1}$. The optimal solution is found after 151 one-shot iteration steps with 40 inner iterations for each of the two adjoint solvers and 80 inner iterations for the primal flow solver. The optimized design has a drag coefficient of $C_D = 3.342 \cdot 10^{-3}$ and a lift coefficient of $C_L = 1.775 \cdot 10^{-1}$. In total, drag was reduced by 29.93%, while lift was almost precisely kept with a relative loss of only 0.67%. The total amount of time needed for each shape update is around 390 seconds including the evaluation of the shape derivative for all $113,956$ design unknowns and one solution of the surface Laplace gradient smoothing operator. The precise timings are shown in table 1. Note that the timings do not exactly add up to 390, as some servicing

Operation	Time in seconds
Volume mesh deformation	36
Dual mesh construction and partitioning	49
Curvature computation	4
Primal flow solver (80 iterations)	101
Adjoint flow solver (drag, 40 iterations)	57
Adjoint flow solver (lift, 40 iterations)	57
Shape derivative evaluation	26
Derivative of volume constraint	4

Table 1. Time spent during each VELA optimization step

steps and the solve with the surface Laplacian are not accounted for. The flow and adjoint solvers were running on four cores of an AMD Phenom II 2.8 GHz PC, while the other steps were computed on one core only.

Looking at figure 5 and the C_P plots in figure 6, one can see that the shock wave on the upper and lower side of the wing could be removed for almost the whole span, while the pressure distribution of the fuselage is also somewhat improved. Observing the airfoil cuts in figure 7, one can see that during optimization, the twist of the wing-fuselage near the root has has slightly decreased, while the twist of the wing near the tip as increased. However, with such a fine parameterization available, the optimizer can achieve a shock-free or almost shock-free aircraft geometry that is very close to the original layout, which appears to be very beneficial for the actual design process, because usually, larger deformations for improving aerodynamics are often problematic from a structural point of view. This is especially true if the actual design process of the aircraft is already in a more advanced state.

VI.   Outlook: Viscous Fluids

The extension of the shape optimization technique presented here to also include viscosity is straight forward and preliminary theoretical studies for the compressible laminar Navier–Stokes equations can be found in.[21] The actual application to viscous compressible fluids is part of current research. The situation becomes somewhat more delicate when turbulent flows are considered. Most of the standard turbulence models have elements for which a formal derivation of the continuous adjoint equation or the partial shape derivative is not straight forward. A good example would be the wall-distance functions of the Spalart–Allmaras turbulence model or some of the boundary conditions in the k-ϵ and the k-ω model. While these difficulties can easily be circumvented by considering a frozen the eddy viscosity, there are also reports of successful uses of analytically adjoined turbulence models.[32] Given the fact that for example the partial derivative of the wall-distance functions or even the complete turbulent flow solver could also be treated
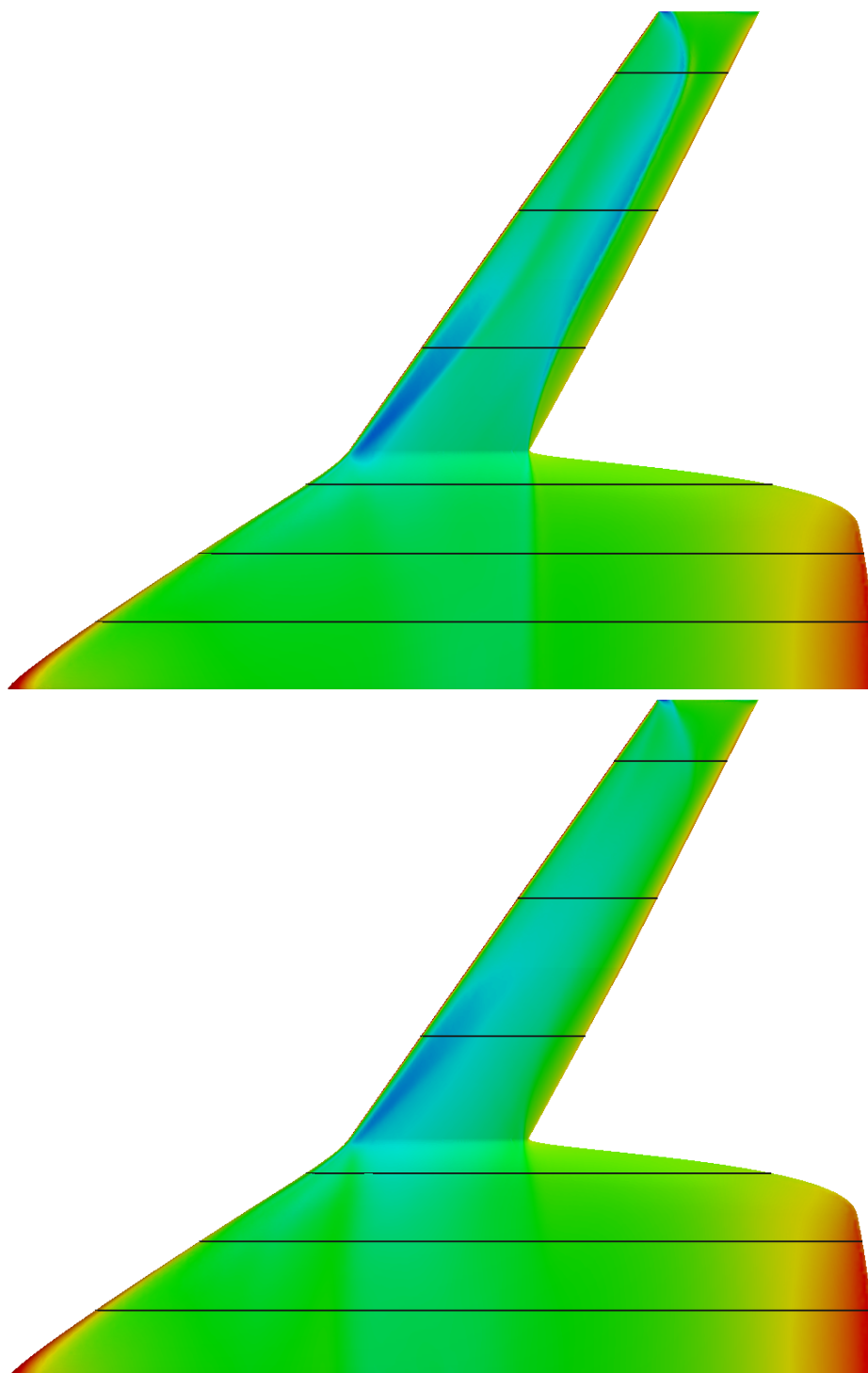
American Institute of Aeronautics and Astronautics

Figure 5. Initial and optimized VELA aircraft. Black lines indicate where the C_P plots and airfoil cuts are computed.

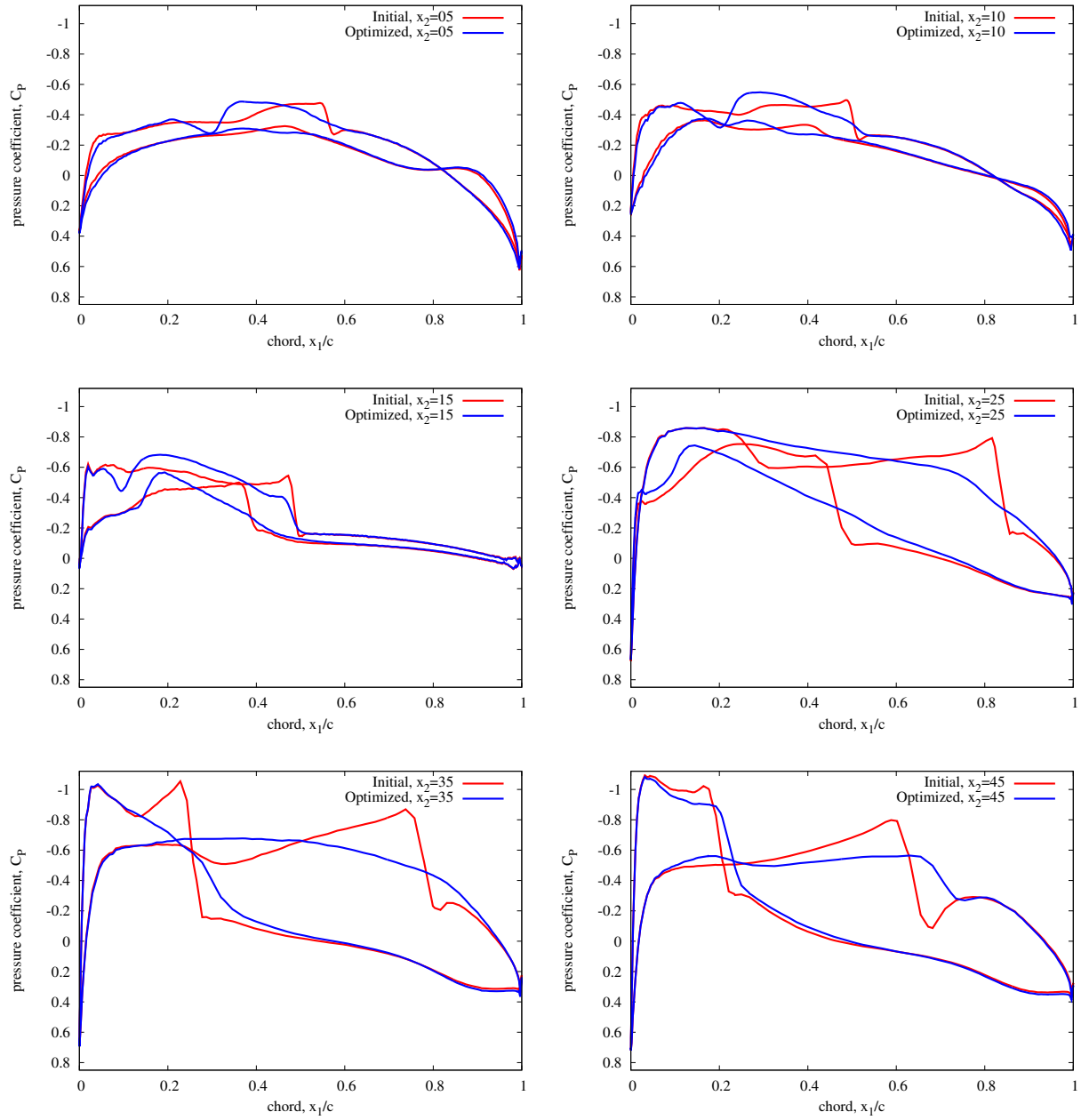American Institute of Aeronautics and Astronautics

Figure 6. Pressure distributions across airfoil cuts for the initial and optimized VELA aircraft. Total span wise extend is $x_2 \in [0, 48.5]$.
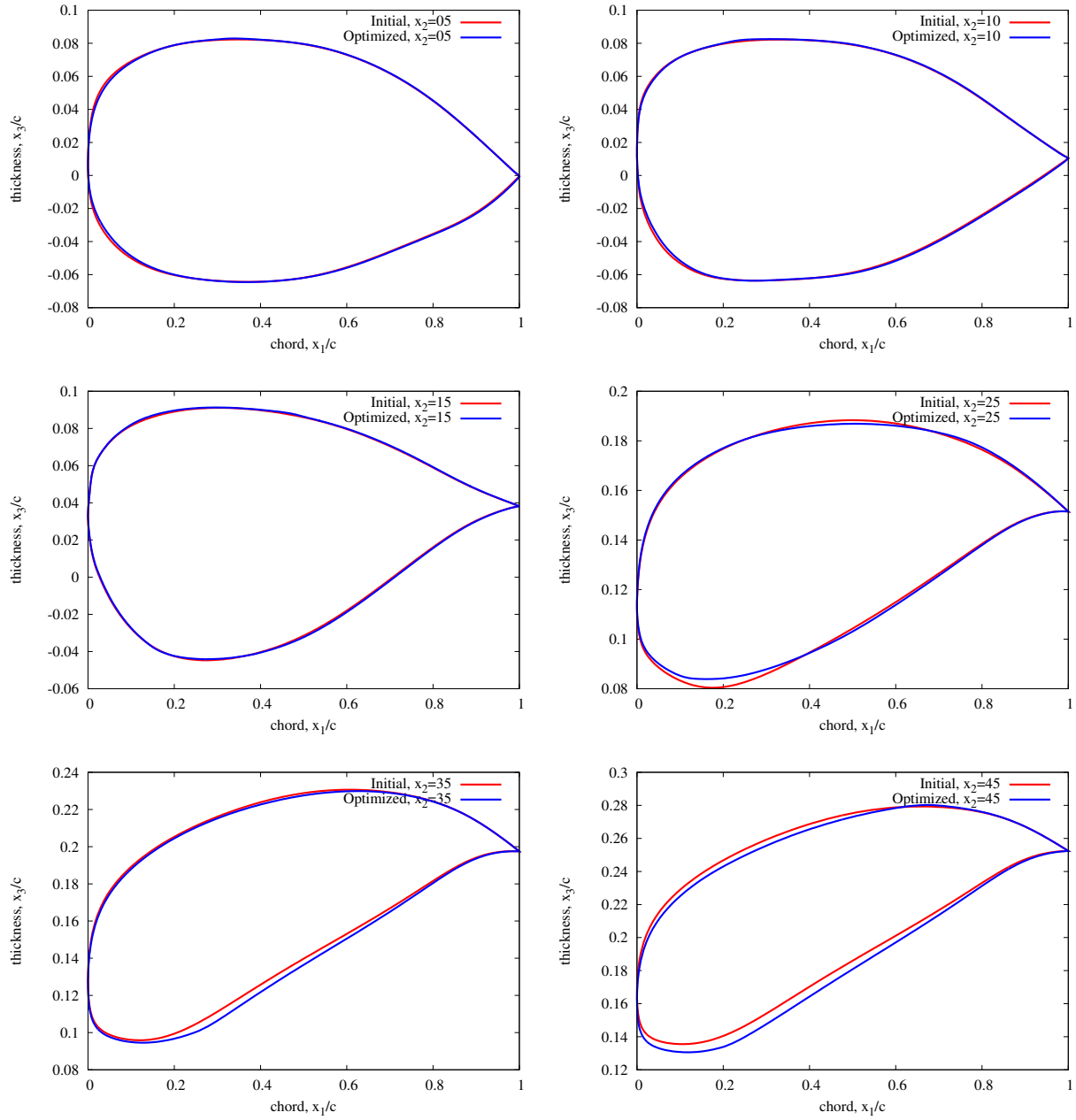
Figure 7. Airfoil cuts for the initial and optimized VELA aircraft. Total span wise extend is $x_2 \in [0, 48.5]$.

American Institute of Aeronautics and Astronautics

efficiently on a discrete level using e.g. algorithmic differentiation,[33] the shape optimization method presented here appears to be also applicable to turbulent flows, although the derivation is probably not straight forward and might require some form of hybridization.

VII.   Conclusions

Large scale aerodynamic shape optimization for the compressible Euler equations in three dimensions is considered. By using the Hadamard form of the shape gradient, a sensitivity information for the aerodynamic forces can be computed extremely efficiently, such that each surface mesh node position can be used as a design parameter. Being an analytic exact surface expression, the partial derivatives of the mesh deformation tool and the mesh sensitivity Jacobians are not required. Using these shape gradients as the reduced gradients in a one-shot optimization strategy creates a shape one-shot method for which the Hessian is approximated using the surface or tangential Laplace operator. Feasibility of the method for large scale aerodynamic problems is shown through the optimization of an Onera M6 wing with $16,792$ unknowns of the shape and the optimization of the VELA blended wing-body concept aircraft using $113,956$ surface mesh node positions as design parameters.

Acknowledgements

References

[1]R. M. Hicks and P. A. Henne. Wing design by numerical optimization. *Journal of Aircraft*, 15:407–412, 1978.

[2]M. Nemec and D. W. Zingg. Towards efficient aerodynamic shape optimization based on the Navier–Stokes equations. In *15th AIAA Computational Fluid Dynamics Conference, AIAA 2001-2532*, Anaheim, CA, June 11-14, 2001.

[3]M. Nemec, D. W. Zingg, and T. H. Pulliam. Multi-point and multi-objective aerodynamic shape optimization. In *9th AIAA/ISSMO Symposium on Multidisciplinary Analysis and Optimization, AIAA 2002-5548*, Atlanta, GA, Sept. 4-6, 2002.

[4]N. Gauger, A. Walther, C. Moldenhauer, and M. Widhalm. Automatic differentiation of an entire design chain for aerodynamic shape optimization. *Notes on Numerical Fluid Mechanics and Multidisciplinary Design*, 96:454–461, 2007.

[5]E. J. Nielsen and M. A. Park. Using an adjoint approach to eliminate mesh sensitivities in computational design. *AIAA Journal*, 44(5):948–953, 2006.

[6]O. Pironneau. On optimum profiles in Stokes flow. *Journal of Fluid Mechanics*, 59(1):117–128, 1973.

[7]O. Pironneau. On optimum design in fluid mechanics. *Journal of Fluid Mechanics*, 64(1):97–110, 1974.

[8]W. Haack. Geschoßformen kleinsten Wellenwiderstandes. *Bericht der Lilienthal-Gesellschaft*, 136(1):14–28, 1941.

[9]C. Castro, C. Lozano, F. Palacios, and E. Zuazua. Systematic continuous adjoint approach to viscous aerodynamic design on unstructured grids. *AIAA*, 45(9):2125–2139, 2007.

[10]B. Mohammadi and O. Pironneau. *Applied Shape Optimization for Fluids*. Numerical Mathematics and Scientific Computation. Clarendon Press Oxford, 2001.

[11]M. C. Delfour and J.-P. Zolésio. *Shapes and Geometries: Analysis, Differential Calculus, and Optimization*. Advances in Design and Control. SIAM Philadelphia, 2001.

[12]J. Sokolowski and J.-P. Zolésio. *Introduction to Shape Optimization: Shape Sensitivity Analysis*. Springer, 1992.

[13]A. Jameson. Aerodynamic design via control theory. *Journal of Scientific Computing*, 3(3):233–260, 1988.

[14]S. Kim. *Design Optimization of High-Lift Configurations Using a Viscous Adjoint-Based Method*. PhD thesis, Stanford University, 2001.

[15]I. Gherman. *Approximate Partially Reduced SQP Approaches for Aerodynamic Shape Optimization Problems*. PhD thesis, University of Trier, Trier, Germany, 2008.

[16]V. Schulz and I. Gherman. One-shot methods for aerodynamic shape optimization. In N. Kroll, D. Schwamborn, K. Becker, H. Rieger, and F. Thiele, editors, *MEGADESIGN and MegaOpt — German Initiatives for Aerodynamic Simulation and Optimization in Aircraft Design*, volume 107 of *Notes on Numerical Fluid Mechanics and Multidisciplinary Design*, pages 207–220. Springer, 2009.

[17]E. Arian and S. Ta'asan. Analysis of the Hessian for aerodynamic optimization: Inviscid flow. Technical Report 96-28, Institute for Computer Applications in Science and Engineering (ICASE), 1996.

[18]E. Arian and V. N. Vatsa. A preconditioning method for shape optimization governed by the Euler equations. Technical Report 98-14, Institute for Computer Applications in Science and Engineering (ICASE), 1998.

[19]A. Jameson, L. Martinelli, and N. A. Pierce. Optimum aerodynamic design using the Navier–Stokes equations. *Theoretical and Computational Fluid Dynamics*, 10:213–237, 1998.

[20]S. Kim, K. Hosseini, K. Leoviriyakit, and A. Jameson. Enhancement of adjoint design methods via optimization of adjoint parameters. In *43rd AIAA Aerospace Sciences Meeting and Exhibit, AIAA 2005-0448*, Reno, NV, 2005.

[21]S. Schmidt. *Efficient Large Scale Aerodynamic Design Based on Shape Calculus*. PhD thesis, University of Trier, Germany, 2010.

[22]S. Schmidt, C. Ilic, N. Gauger, and V. Schulz. Shape gradients and their smoothness for practical aerodynamic design optimization. Technical Report Preprint SPP1253-10-03, DFG-SPP 1253, 2008. (submitted to OPTE).

[23]S. Schmidt and V. Schulz. Impulse response approximations of discrete shape Hessians with application in CFD. *SIAM Journal on Control and Optimization*, 48(4):2562–2580, 2009.

[24]S. Schmidt and V. Schulz. Shape derivatives for general objective functions and the incompressible Navier–Stokes equations. Technical Report Preprint SPP1253-10-05, DFG-SPP 1253, 2009. (submitted to Control and Cybernetics).

[25]K. Eppler, S. Schmidt, V. Schulz, and C. Ilic. Preconditioning the pressure tracking in fluid dynamics by shape Hessian information. *Journal of Optimization Theory and Applications*, 141(3):513–531, 2009.

[26]N. Gauger. Das Adjungiertenverfahren in der aerodynamischen Formoptimierung. *DLR Forschungsbericht*, 2003-05, 2003.

[27]M. B. Giles and N. A. Pierce. Adjoint equations in CFD: duality, boundary conditions and solution behaviour. *AIAA*, 97-1850, 1997.

[28]S. Rusinkiewicz. Estimating curvatures and their derivatives on triangle meshes. In *Symposium on 3D Data Processing, Visualization, and Transmission*, 2004.

[29]K. Eppler and H. Harbrecht. A regularized Newton method in electrical impedance tomography using shape Hessian information. *Control and Cybernetics*, 34(1):203–225, 2005.

[30]M. Hintermüller and W. Ring. A second order shape optimization approach for image segmentation. *SIAM Journal on Applied Mathematics*, 64(2):442–467, 2004.

[31]L. D. López Pérez. *Régularisation d'images sur des surfaces non planes*. PhD thesis, Université de Nice–Sophia Antipolis, 2006.

[32]A. S. Zymaris, D. I. Papadimitriou, K. C. Giannakoglou, and C. Othmer. Continuous adjoint approach to the Spalart–Allmaras turbulence model for incompressible flows. *Computers & Fluids*, 38:1528–1538, 2009.

[33]A. Carnarius, F. Thiele, E. Özkaya, and N. Gauger. Adjoint approaches for optimal flow control. *AIAA*, 2010-5088, 2010.